Load monitoring of aerospace structures utilizing micro-electro-mechanical systems for static and quasi-static loading conditions

2012 Smart Mater. Struct. 21 115001

(http://iopscience.iop.org/0964-1726/21/11/115001)

Smart Mater. Struct. **21** (2012) 115001 (11pp) doi:10.1088/0964-1726/21/11/115001

Load monitoring of aerospace structures utilizing micro-electro-mechanical systems for static and quasi-static loading conditions

M Martinez, B Rocha, M Li, G Shi, A Beltempo, R Rutledge and M Yanishevsky

National Research Council Canada, Institute for Aerospace Research, 1200 Montreal Road, Ottawa, ON, K1A 0R6, Canada

E-mail: Marcias.Martinez@nrc-cnrc.gc.ca

Received 19 December 2011, in final form 17 July 2012
Published 14 September 2012
Online at stacks.iop.org/SMS/21/115001

Abstract
The National Research Council Canada (NRC) has worked on the development of structural health monitoring (SHM) test platforms for assessing the performance of sensor systems for load monitoring applications. The first SHM platform consists of a 5.5 m cantilever aluminum beam that provides an optimal scenario for evaluating the ability of a load monitoring system to measure bending, torsion and shear loads. The second SHM platform contains an added level of structural complexity, by consisting of aluminum skins with bonded/riveted stringers, typical of an aircraft lower wing structure. These two load monitoring platforms are well characterized and documented, providing loading conditions similar to those encountered during service.

In this study, a micro-electro-mechanical system (MEMS) for acquiring data from triads of gyroscopes, accelerometers and magnetometers is described. The system was used to compute changes in angles at discrete stations along the platforms. The angles obtained from the MEMS were used to compute a second, third or fourth order degree polynomial surface from which displacements at every point could be computed. The use of a new Kalman filter was evaluated for angle estimation, from which displacements in the structure were computed. The outputs of the newly developed algorithms were then compared to the displacements obtained from the linear variable displacement transducers connected to the platforms. The displacement curves were subsequently post-processed either analytically, or with the help of a finite element model of the structure, to estimate strains and loads. The estimated strains were compared with baseline strain gauge instrumentation installed on the platforms. This new approach for load monitoring was able to provide accurate estimates of applied strains and shear loads.

(Some figures may appear in colour only in the online journal)

1. Introduction

Scientists and engineers at the National Research Council Canada (NRC) Institute for Aerospace Research (IAR) have been developing a new capability using micro-electro-mechanical systems (MEMS) with the intent of performing in-flight load monitoring. The measurement of aircraft operation loads is an expensive task required for certification and for determining remaining useful component lives. Currently, during the development of a new aircraft, measured values of flight (manoeuvre/gust) and ground loads are required to check and validate the calculated design loads

of the aircraft. In some cases, the design and fatigue loads used in original equipment full scale certification tests have been found to be substantially different from the way aircrafts are actually being used in service [1]. To overcome these shortfalls and increase aircraft safety, as well as provide vital information for aircraft operators and maintainers, continuous flight load measurements with comparisons to static strength and fatigue flight envelope test data would be ideal and could result in considerable cost savings for future generations of aircraft.

Operational flight load measurements are currently accomplished by acquiring strain, flight parameters (pitch, roll, yaw, accelerations and rates, control surface deflections, altitude, air speed, angles of attack, etc), and '*g*' acceleration. The use of accelerometers to measure loads is well documented in the literature [2]. To determine structural loads, the three dimensional components of acceleration are integrated twice to determine position, and from the position (deformation), loads can be calculated. However, the integration process is prone to numerical errors lowering the signal to noise ratio (SNR). Strain gauges are also installed on aircraft structural components for strain and subsequent load monitoring in a small number of flight tests and ground tests, where known loads are applied at specific locations [3]. From the generated data and the known loading geometry, predictive loading equations are generated that are sufficient to calculate the bending moments, shear loads and torsion moments on the structure of interest. Complete validation of these loading equations requires the use of accelerometers to measure inertial loads, as well as the measurement of additional relevant flight parameters (such as altitude) for verification against the design flight regime 'points in the sky' established during flight testing [4]. The Royal Canadian Air Force (RCAF) also followed this requirement and developed computer algorithms which separated the effects of manoeuvres and gusts [5].

In flight test aircraft, many strain gauges are utilized to generate the response equations. Load monitoring systems based on strain gauge sensors present, however, certain problems such as: the gauges themselves become damaged by fatigue; they require complex wiring networks to be installed and maintained, to enable the use of all necessary sensors [6]; the endurance and reliability of strain gauges and their electrical circuitry, electrical contacts, wiring and bonding may deteriorate over the long term; and the electro-magnetic interference (EMI) that strain gauge sensor systems may generate and be sensitive to. The mentioned problems and reliability have been consistently observed both in flight tests and in full scale fatigue tests, and have led many aircraft manufacturers, operators and maintainers to avoid considering such flight load monitoring at all. This justifies required research and development of load monitoring systems based on different sensor types.

MEMS are micromachines/mechanisms driven by electricity, capable of acting as actuators and sensors. With the rapid growth of consumer electronic technologies, the price of MEMS has dropped substantially and their application has widely increased to the extent that MEMS are now found in game consoles, inkjet printers, smart phones, and industrial and biomedical pressure sensors, to name a few [7, 8]. In the application of MEMS as sensors, engineers and scientists have been able to incorporate accelerometers (measuring three degrees of freedom), gyroscopes, magnetometers, and temperature sensors into a single compact unit with dimensions on the order of 40 mm × 40 mm × 15 mm.

Only a small number of studies have been reported in the literature regarding the process of estimating loads from the measured deformation of a structure based on sensors such as: fibre optic or regular strain gauge sensors [9]. Similarly, the use of MEMS for load monitoring has been reported in only a small number of publications. For example, the use of MEMS and fibre optic sensors in combination with accelerometers and inclinometers for load monitoring of civil structures was proposed in [10]. Lee in [11] proposed the use of MEMS to measure strain, by using a micromechanism based on the measurement of the distance between two micro-plates attached to a structure. In [12], the use of MEMS accelerometers to measure the vibrations in the cables of a suspension bridge, enabling the subsequent calculation of the applied loads, was studied. It is the novel combination of the use of MEMS and deformation of the structure as a load monitoring technique that is being considered in this study for aerospace applications.

2. Methodologies

The approach utilized in this research focuses on distributing MEMS sensors along a structure in order to monitor its deformation. This can be achieved using MEMS, since they are capable of capturing the changes in angles/orientation at every sensor location. A polynomial fitting of these angles is applied from which continuous spatial deformation of the structure is obtained, enabling the computation of applied loads using either analytical methods or finite element methods (FEM). This novel approach towards load monitoring avoids the many complications encountered in using strain gauges and the identification of strain along an entire span of the structure versus specific strain measurements at specific locations. An analytical approach could potentially be used for simple structures, loading and boundary conditions, where a closed form analytical solution is available. Since complex structures can be decomposed into simpler, elemental structures with simpler loading and boundary conditions, a study into simpler structures and conditions provides the foundation for load monitoring of more complex structures.

A more general approach makes use of numerical techniques, such as FEM. From the deformation of the structure, and by assuming a quasi-static or static condition, FEM can be applied to compute the applied loads (strain and stresses) following the contour method approach [13, 14], which makes use of linear elastic FEM, represented by equation (1).

$$F = K\bar{x} \tag{1}$$

where F is the applied nodal load; K represents the global stiffness matrix of the structure; and $\bar{x}$ represents the nodal

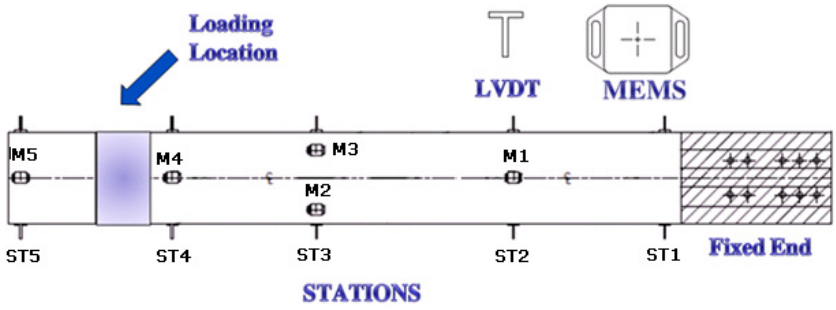

Figure 1. SHM Platform 1-A—MEMS and LVDT stations.

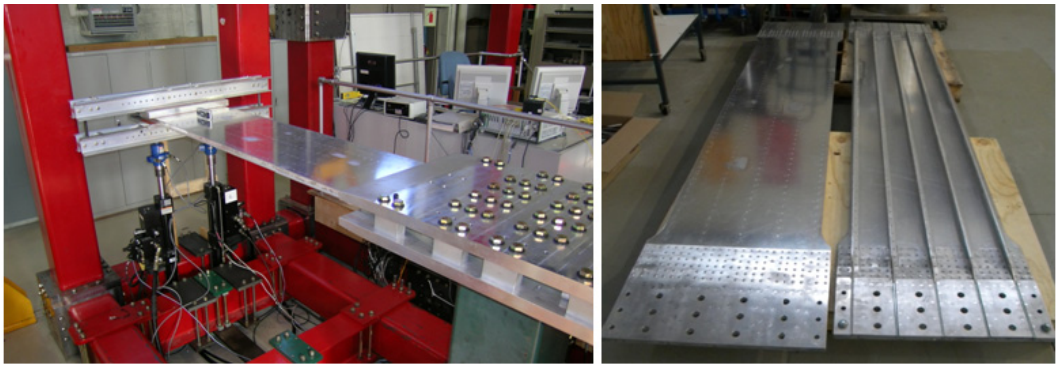

Figure 2. Platform 1-B (left) side view of the platform and actuators (right) top and bottom view.

displacement vector. The $\bar{x}$ displacement can be obtained at any point along the beam if a theoretical deflection curve is obtained from directional cosines (changes in angles) measured by the MEMS. It is important to note that MEMS data and changes in angles alone are only sufficient if the small strain theory approximation is valid. If the change in the geometry of the structure is significant, then the actual displacement of the MEMS node will be required. This can be potentially achieved by using the accelerometer data from the MEMS to compute the initial and final position within a specified time window. For the case of more complex structures, such as real aircraft wings with varying geometries along their length, the stiffness of the structure can be calculated from FEM [15, 16]. The estimation of loads/strains using the FEM in this study was performed on a more complex structure using MSC/PATRAN as the pre- and post-processor and ABAQUS as the solver.

3. Test setup

NRC-IAR has developed a family of platforms for assessing structural health monitoring (SHM) and load monitoring systems. These structural facilities range in complexity from basic structural components to an actual wing from a CF-188 fighter aircraft. The primary objective when designing the platforms was to assist in the development of load monitoring systems transitioning from a full scale test environment, as presented in this manuscript, to future flight operational service on an aircraft.

The first platform being considered in this manuscript, referred to as 'Platform 1-A', consisted of two symmetrical rectangular aluminum cantilevered beams with hydraulic actuators on each extremity for load application. Each cantilever beam measured approximately 2.7 m in length (per side), for a total length of approximately 5.5 m, mimicking an aircraft wing spar. The loading on the rectangular beam structure was applied at 2.04 m from the root, perpendicularly to the beams' plane. Both the leading and trailing edges of one of the cantilever beams were instrumented with linear variable displacement transducers (LVDTs), as shown in figure 1. The other ends of the LVDTs were fixed to a reaction frame, which enabled the measurement of the linear deformation of the beam relative to a static reference plane. For the purpose of this study, LVDTs are considered the "gold standard" for laboratory testing, giving the measurements to which all other displacement type sensor outputs are compared to. On the upper side of the cantilever beam, a series of MEMS were strategically located at five stations along the length of the beam as seen in figure 1. In the case of Station 3, two MEMS sensors were located in line with each other for sensing any torsion applied to the beam. However, it is important to note that in this study, bending was only considered as a first attempt in obtaining the loading conditions from MEMS on a simple structure. The benefit of this simple structure is that the analytical classical Euler–Bernoulli beam theory can be applied for initial evaluation of this novel load monitoring technique [17].

The second SHM platform (hereafter 'Platform 1-B') consisted of an aluminum reinforced skin with riveted stringers (stiffened shell/plate), as shown in figure 2. This platform represents a higher level of structural complexity. SHM Platform 1-B is also 5.5 m in length with a width

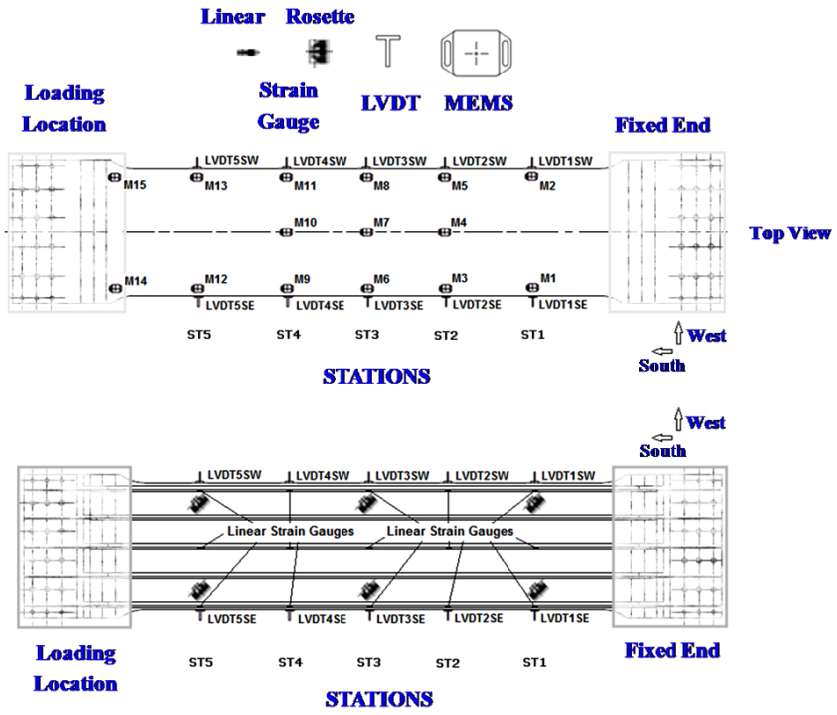

Figure 3. Instrumentation on SHM Platform 1-B.

of 0.505 m. The skin of this second platform is made of aluminum alloy 7075-T6, while the stringers are made of aluminum alloy 2024-T3. The primary purposes of this second platform are to evaluate the ability of the MEMS sensor to capture deformation of a more complex structural component and determining the strains and stresses sensed by the structure via a finite element (FE) model.

The MEMS used in this study were acquired from GLI Interactive LLC. These MEMS were selected due to their compact size and their ability to provide data from embedded accelerometers, gyroscopes, magnetometers and temperature sensors. A total of five MEMS were strategically located along the length of SHM Platform 1-A (figure 1), while 15 MEMS were strategically located along the length of SHM Platform 1-B (figure 3) in order to obtain real time angle changes at each station during structural deflection. The MEMS are capable of outputting an orientation quaternion, Euler angles, and temperature data at frequencies as high as 100 Hz. The gyroscopic data obtained from the MEMS sensor are provided in the form of quaternions. A detailed introduction to quaternion math can be found in [18].

The applied load for both platforms consisted of a quasi-static load condition with a stepped ramp using 0.0127 m increments of actuator displacement applied during five second intervals, with step holds of three seconds at the end of each increment. The test article consisting of SHM Platform 1-A was bent upwards, with actuators reaching a peak positive displacement of 0.1016 m, then bent downwards to reach a peak negative displacement of −0.0508 m, before returning to zero with the specimen returning to its original undeformed shape. In the case of SHM Platform 1-B, the applied load also consisted of a quasi-static loading condition with a peak positive displacement of 0.0508 m and a peak negative displacement of −0.0254 m.

4. Results

4.1. Results on SHM Platform 1-A

Due to the simple nature of the rectangular beam representation of a wing structure under study, it was possible to estimate the deflection of the beam using the Euler–Bernoulli beam in bending analytical theory. The maximum tip deflection ($v_{\max}$) as well as the deflection as a function of position along the length/span of the beam (x) can be found in many standard textbooks on engineering mechanics, such as [17], and these are given below in equation (2):

$$v_{\max} = \frac{PL^3}{3EI}$$
$$v = \frac{P}{6EI}(2L^3 - 3L^2x + x^3) \tag{2}$$

where P is the applied point load; L is the length of the beam between its fixing station and the load application station; E is Young's modulus of the beam material; and I is the moment of inertia. The parameters at peak positive displacement can be found in table 1.

From equation (2), the maximum estimated theoretical deflection was computed to be 0.105 m, which matched closely the deflection at the load application location measured by the load control system LVDT (0.102 m). Figure 4(a) shows a comparison of the vertical displacement along the length/span of a beam obtained from equation (2)

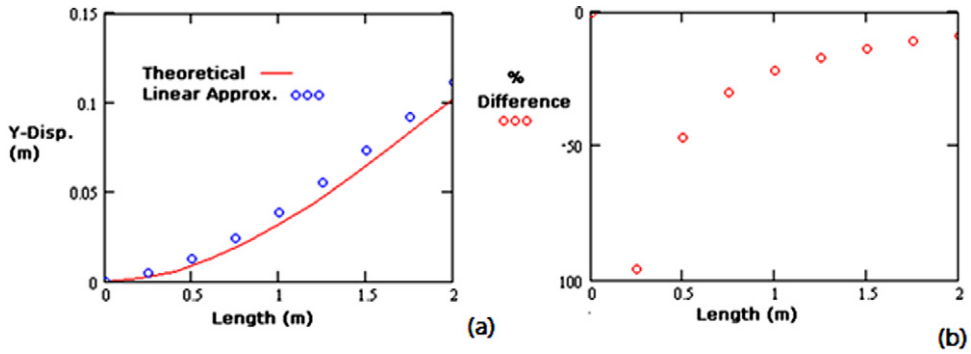

Figure 4. (a) Displacement comparison—theoretical versus linear approximation; (b) error estimation (% difference).

Table 1. Beam/wing parameters.

Parameter	Value	Units
P—Applied point load	1085.0	N
L—Length of the beam	2.04	m
E—Young's modulus	70.0	GPa
b—Base of the cross sectional area of the beam	0.3048	m
h—Height of the cross sectional area of the beam	0.0254	m
I—Moment of inertia ($bh^3/12$)	4.16×10^{-7}	m^4

and its corresponding linear approximation computed from the slopes (the first derivative with respect to x of equation (2)) assuming a spacing of 0.25 m between points. It has been very well described in the literature that an incremental (Euler) approximation will always diverge, thus the need for a non-linear solution method such as the iterative Newton–Raphson method [19]. As spacing between points is reduced, the incremental (Euler) approximation converges to the theoretical solution, thus the need for a higher order approximation from the polynomial fitting that will be obtained from discrete MEMS sensors.

It is important to note that a linear approximation close to the root of the beam (cantilever end) produced a very large error (percentage difference) with respect to the theoretical solution, as shown in figure 4(b). This preliminary theoretical result indicates that at the constrained end of the beam, it may be appropriate to use other means of estimating displacement. However, it is important to note that although the theoretical percentage difference at the root of the beam may be large, the overall magnitude of the difference between the Euler linear approximation and the theoretical solution is small.

In our experiment the LVDT data provided the overall vertical displacement of the beam with respect to its reference or undeformed state. These data were used to compute the angle at each LVDT station. Since the form of the Euler–Bernoulli equation for the deflection of a cantilever beam yields a third degree polynomial as a solution, a polynomial of the same order was fit tested to the discrete displacement data from the LVDT sensors. Since the data derived from the MEMS consist of beam slopes, the derivative of the third degree polynomial curve (fit to the LVDT data) was calculated and compared to the data from the MEMS to

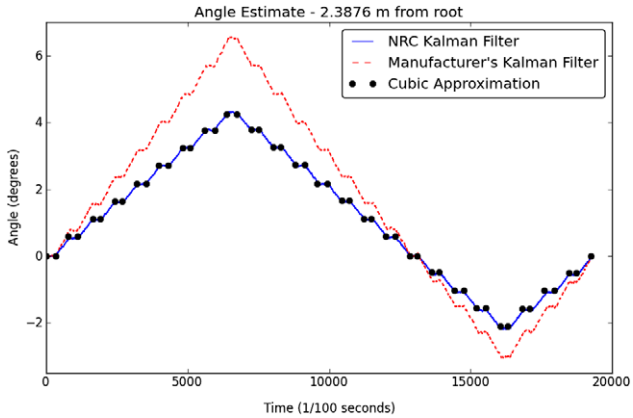

Figure 5. Computed angles from MEMS at Station 5.

provide a baseline between the two sensor systems (LVDTs versus MEMS). Figure 5 shows the computed angles (slopes) from the MEMS at Station 5 during the execution of one test with the application of different bending loads. In this figure, several trends are shown and verified with respect to the derivative of the cubic polynomial constructed from the LVDT data (the circular dots in the figures). The angular data from each MEMS sensor, as represented in figure 5 by the broken line, were obtained from the Kalman filter provided by the MEMS manufacturer. The initial results lead us to consider the development of a custom Kalman filter for this application, whose improved performance is shown by the solid line denoting the values obtained using the NRC Kalman filter in figure 5.

The results shown in figure 5 clearly demonstrate why a custom Kalman filter had to be developed, as the MEMS manufacturer's filter tended to overshoot the angles. The NRC developed custom filter (based upon the extended Kalman–Bucy architecture) [20] was found to accurately monitor changes in angles particularly well for the quasi-static scenario. It is foreseeable that as more dynamic load scenarios are tested, the developed NRC custom filter will need some fine adjustments to provide better estimates.

The greatest drawback with the analytical method was that it required a closed form solution for the structure in question. Although this is an efficient approach in the current

case, it can be very challenging to obtain, particularly in the case of a complex structure, such as the CF-188 wing.

4.2. Estimation of strain and shear forces from MEMS data

The strains and shear forces in the rectangular constant cross section aluminum beam subjected to bending were estimated using MEMS/slope data. To arrive at these estimates, the MEMS readings were first post-processed using the NRC-IAR developed custom filter (based upon the extended Kalman–Bucy architecture), and then computed over the length/span of the beam. This computed slope curve was then differentiated using the Euler–Bernoulli beam theory differential equation, with the first derivative (of the rotation/slope given by the MEMS) yielding strain/moment, and the second derivative yielding shear. Under the appropriate boundary conditions, this inverse problem is well characterized and the computed slope curve should correspond to a forcing function matching the experimental load distribution. However, in practice it was found that the resulting load estimates were strongly affected by the behaviour of the applied fitting method, particularly in the differentiation of its resulting fitting curve. For example: a cubic spline interpolant was attempted; however, it introduced inflections between data points, thereupon causing each successive derivative (i.e. strains and shear forces) to fluctuate, when in reality they should have been smooth. It was found that using a piecewise least squares fitting polynomial avoided these issues and yielded excellent results compared to strain gauge measurements and theoretical predictions. The optimal order of this polynomial fit was determined using a statistical test known as ANalysis Of VAriance (ANOVA), as explained in the next section. The optimum polynomial order predicted by ANOVA was found to agree with the order, as predicted by Euler–Bernoulli beam theory.

4.3. Constrained piecewise least square fit

Rather than modelling the slope of the beam as a single continuous function, a piecewise function split between two domains was considered instead. One section of this piecewise function encompassed the root to the load applicator, while the other covered the remaining span from the load applicator to the tip of the beam. In both sections, a least squares fitting polynomial was constructed from corresponding MEMS data to compute the slope curve over the entire beam length. Although these two curve fitting problems could be solved independently, two constraints that reflected the state of the physical system were imposed to relate them together. The first constraint ensured that the computed slope curve was continuous along the beam by forcing each piecewise fit to hold the same value where they intersected (continuity). Similarly, the second constraint guaranteed continuity in the estimated moment distribution by enforcing the same condition to each piecewise derivative. In addition, two boundary conditions befitting a cantilever beam were imposed to enable the inverse Euler–Bernoulli problem to be solved.

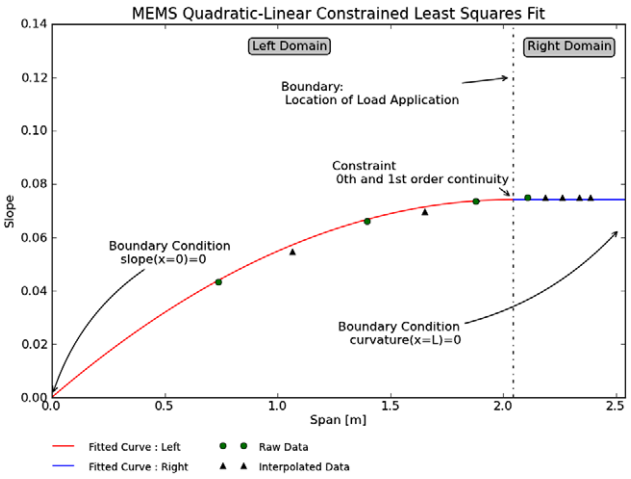

Figure 6. Slope versus span of a cantilever beam.

These boundary conditions constrained the beam to have zero slope at the root, and zero curvature at the free end.

In figure 6, the dotted vertical line illustrates the boundary between domains (also known as the location of the load applicator), while the points represent the slope data recorded by the different MEMS sensors installed along the span of the structure, at the different stations, as shown in figure 1. To increase the solution space, the number of MEMS was artificially augmented, as indicated by the triangular points in figure 6. The additional points were required in order to have enough data points to test higher order polynomial approximations. The additional points in the left domain region correspond to linear interpolations of the data obtained from the two adjacent sensors. In the second region, the augmented triangular points were artificially added, having the same slope (change in slope equal to zero) as the one obtained by the MEMS sensor at Station 5, as indicated in figure 1.

The remaining task to the MEMS data fitting problem was to identify a suitable polynomial fit order for each segment. The coefficient of determination (R^2) value proved to be an inadequate statistic as it favoured higher ordered polynomials, when in practice lower ordered models were more accurate. Typically, in unconstrained polynomial regression, the order would be determined using two ANOVA statistical tests [21]. The first ANOVA test would evaluate whether or not the particular polynomial fit appropriately captured the variance of the test data. If this criterion is met, then a second test would be needed to determine whether increasing the polynomial order significantly captures more of the data's variance. It is insufficient to simply rely on the first test, since once it is passed, any polynomial with a higher degree would be guaranteed to pass. To the authors' knowledge, there has not been any study regarding an analogous statistical test for identifying the appropriateness of constrained segmented polynomial regressions. The closest published work that broaches this topic was performed by Gallant and Fuller in [22], where they proposed an ANOVA test for their segmented first order continuous, but unconstrained, polynomial model. Utilizing

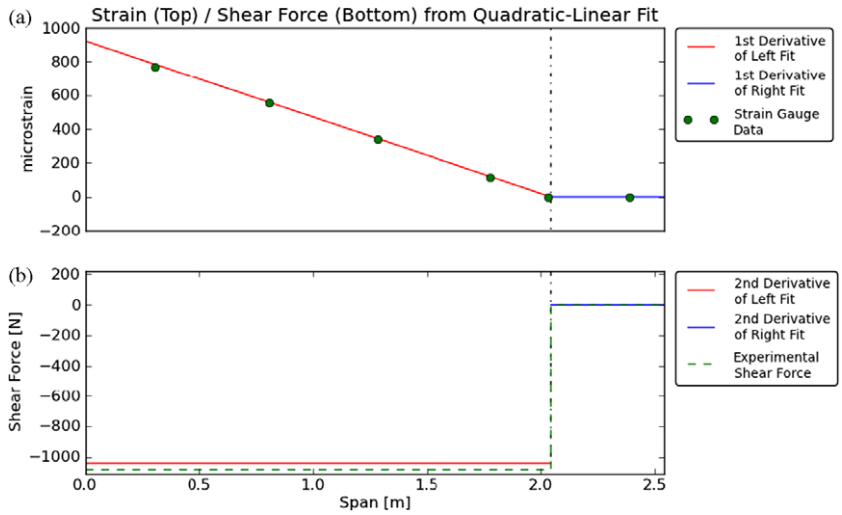

Figure 7. (a) Strain versus span of a cantilever beam—Platform 1-A; (b) shear force versus span of a cantilever beam—Platform 1-A.

a similar approach and understanding that the ANOVA tests were originally designed for unconstrained regressions, the ANOVA tests were applied to each region of the MEMS data.

It was found that the initial test to determine the appropriateness of the polynomial fit was sufficient to identify the order of the segmented polynomial. The results demonstrated that the MEMS data would be best represented by a quadratic–linear model (respectively on the left–right domains), which is in accordance with the theoretical results of the slope of a beam subject to a point load, using the Euler–Bernoulli beam theory. Unlike unconstrained regression, the higher order models did not pass this test, a phenomenon likely owing to the influence of the problem constraints. Figure 7(a) shows the resulting strain curve computed from the MEMS data, which corresponds well to the strain gauge data obtained at the different stations on the cantilever beam, indicated by the solid dots in the figure. Figure 7(b) shows the corresponding shear force obtained from the MEMS data and its validation with respect to the load applicator data acquisition system.

Mathematically, the procedure used to identify the polynomial order was performed as follows. For each segment in the domain, the sum of the square of regression (SSR) and the sum of squares of deviation (SSD) are calculated as shown in the equations below:

$$\mathrm{SSR} = \sum_i (\widehat{Y}_i - \bar{Y})^2 \tag{3}$$

and

$$\mathrm{SSD} = \sum_i (\widehat{Y}_i - Y_i)^2 \tag{4}$$

where $\widehat{Y}_\mathrm{i}$ denotes the regression estimate at X_i, $\bar{Y}$ is the arithmetic mean of the observed data set, and Y_i are the individual observations.

Secondly, the ratio of the mean squares is calculated as follows:

$$\left(\frac{\mathrm{SSR}}{\mathrm{SSR}}\right)\left(\frac{N-M-1}{M}\right)^{-1} \tag{5}$$

where M is the polynomial order and N is the number of data points.

Finally, this ratio was compared to the F distribution with degrees of freedom M and N–M–1, with a confidence value of 95%. If the ratio is within the F statistic, then it could be claimed (with 95% confidence) that the polynomial order sufficiently represented the data.

4.4. Results on SHM Platform 1-B

As the F-test is a statistical method, it is unrealistic, and indeed impossible, to expect it to arrive at the correct polynomial fit one hundred per cent of the time. In the instances where it does go awry, it may return a polynomial order that is higher or lower than what the physical situation dictates. Consequently, it is vital to understand what repercussions a higher order parameterization may have towards the determination of loads and strains. To investigate this, a FE simulation was conducted on SHM Platform 1-B, which has a more involved cross sectional geometry, and whose dynamics may not be captured by the Euler–Bernoulli formulation completely.

Once the FE model is provided with a parameterization of the deformation surface obtained from the integration of the fitted surface to the MEMS data, a numerical solution for strains and stresses, based on the FEM, can be calculated. For the purpose of this study, the deformation surface curve was taken to be one dimensional since only the bending mode was investigated, with this being the primary loading condition on an aircraft wing, followed by torsion and shear. These surface curves were constructed by fitting a spanwise second, third and fourth order curves to the MEMS output, and subsequently integrated to arrive at the surface displacement curve. The results in figure 8 demonstrate that, despite the variation in order, the resulting displacement curve from each parameterization yields very close results. Indeed, even if Euler–Bernoulli were naively applied, the difference in the predicted displacement is small, as shown in figure 8.

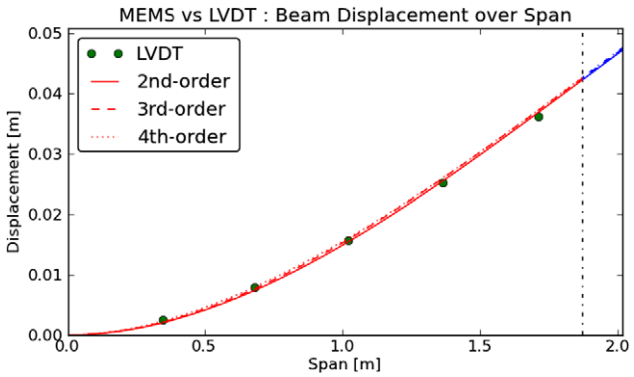

Figure 8. SHM Platform 1-B—MEMS versus LVDT displacement.

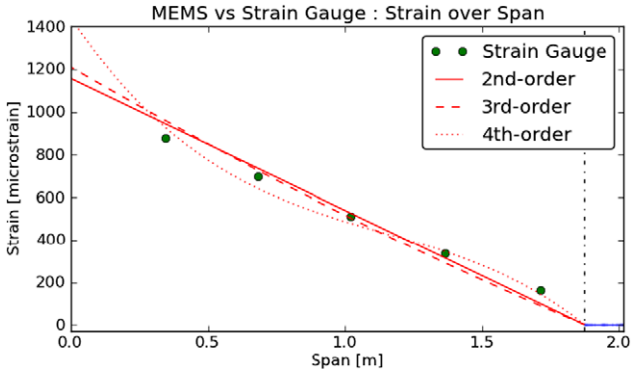

Figure 9. Platform 1-B: MEMS versus strain gauges using Euler–Bernoulli's approach.

The vertical dotted lines in both figure 8 and figure 9, at approximately 1.8 m from the root of the structure, correspond to the region where the clamping mechanism that is connected to the load applicator on SHM Platform 1-B begins, as shown in figure 10.

Figure 9 shows that the numerical results from Euler–Bernoulli's approach match very closely those from the strain gauge readings. As seen in this figure, the results from this approach match not only in value but also the strain distribution, especially when a fourth order curve was considered.

Table 2 shows the results, in terms of strains, obtained from the application of different parameterization curves on a FE model of SHM Platform 1-B. Not shown in this table is the comparison between the predicted strain along the stringers and the actual measured strain. Since these Z stringers deform non-linearly with the beam (due to asymmetry and subsequent bending induced torsion and warping), the Euler–Bernoulli theory yields very inaccurate strain results. However, with the FE model (as shown in figure 10 (a)), it is possible to compute the strain on the stringers. These results are promising, as they indicate how this method can be applied to structures with complex geometries, without the strict need to obtain and use the proper parameterization curve in all sections of the model. As seen in table 2, a fourth order slope fitted curve applied to the FE model produces strain values that fall between a 2.8 to 10.4% difference from the measured strain results. This result may suggest that SHM Platform 1-B may be described as a fourth order system.

One of the key advantages to the FE approach that we are suggesting in this study is the ability to determine the complete strain and stress behaviour of a complex structure by measuring the slopes resulting from the deformation of the structure, through the use of MEMS sensors. Our FE model was developed with 8-node hexahedron (brick) elements and a total of 39 269 elements and 67 900 nodes were assigned. In figure 10(a), the strain fringe obtained from the FE model, for a statically applied bending load, for SHM Platform 1-B, is presented. As seen in this figure, from the use of a representative FE model, information on the strain distribution on the stringers is also obtained, even though the applied deformation field in the model was only applied to the skin of the structure. A key aspect to this approach is the need for the development of an accurate representative model of the structure, including its material properties and behaviour.

Figure 10(b) shows the spanwise strain profiles for SHM Platform 1-B, along its centre section. These strain profiles

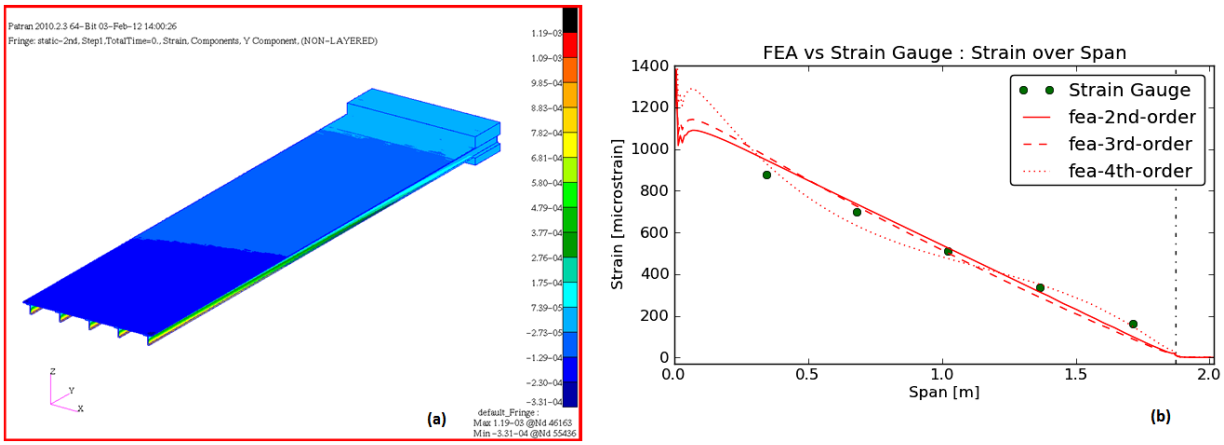

Figure 10. (a) SHM Platform 1-B strain distribution results for second order MEMs polynomial from FEM; (b) strain profile curve from the FE model versus measured strain gauge data.

Table 2. Experimental versus FEA parameterizations (microstrain).

Stations	Strain gauge	Second order FEA (% Diff.)	Third order FEA (% Diff.)	Fourth order FEA (% Diff.)
ST1	877.4	932.2 (6.2%)	949.5 (8.2%)	914.3 (4.2%)
ST2	696.1	727.1 (4.5%)	716.8 (3.0%)	624.0 (−10.4%)
ST3	511.2	520.9 (1.9%)	496.3 (−2.9%)	469.7 (−8.1%)
ST4	336.6	309.4 (−8.0%)	284.6 (−15.4%)	345.9 (−2.8%)
ST5	163.3	98.2 (−40.0%)	86.7 (−47.0%)	146.4 (−10.3%)

were obtained from the FE model when the parameterization curves of different order were used as input to the model. To serve as a baseline for comparison of the FE data, the strain gauge data obtained experimentally for the same loading condition is also presented in figure 10(b). In the proximity of the root of the FE model, a discontinuity in the FE strain results can be seen. These discontinuities are the result of imposed clamping at the root of the structure in our FE model.

5. Discussion

The use of a MEMS based sensor system for load monitoring has been shown to produce results that closely match data from load cells, LVDTs and strain gauges used to gather reference data in experimental setups. Allocating the minimum number of MEMS to each region of the domain required prior knowledge of the load application location for the case of the analytical approach methodology, demonstrated in SHM Platform 1-A. However, the results on SHM Platform 1-B, which also closely matched measured reference data for the experimental setup, made use of the accuracy of the FE model in combination with the deformation surface produced by integrating the fitted spatial distributions to MEMS sensors' slope data. The use of Euler–Bernoulli's beam in bending theory requires the structure and loading to be divided in different domains, separated in the locations where discontinuities occur either in the loading condition—point loads, breaks, etc—, or in the structure—changes in rigidity, Young's modulus, geometry/cross section, etc, such as reinforcements. Clearly, these discontinuity conditions would subsequently affect the order of the applied best-fit polynomial. In the case of Platform 1-A, the division between sections was intentionally placed coincident with the load applicator, as the load applicator induced a discontinuity in the shear force. Since the constraints to the fit only required continuity in slope and moment, the second derivative (shear) of the fit was free to also be discontinuous at the same location. If instead a single continuous function spanning the entire length of the beam was pursued for modelling, it would inevitably encounter difficulties capturing the shear behaviour, since a smooth function could never truly approximate a step function. In practice, locating these discontinuities in shear on a real aircraft wing (and thus the divisions) would be a matter of identifying: the location of the pylons, to which missiles, external pods, cargo and engines attach; the location of the beginning and end of fuel tanks, or aerodynamic elements, such as flaps, ailerons, etc, or even structural components, reinforcements and wing breaks. Should one or more discontinuities arise, as in the case of the application of an analytical approach to a wing structure, the number of divisions/domains, determining also the required number of MEMS, could easily be recalculated and the analytical (fitting) problem could be reformulated as a constrained least squares fit over M piecewise domains, with similar constraints for slope and curvature continuity enforced over each domain boundary.

The FE approach demonstrated in SHM Platform 1-B provided very accurate results despite the increased complexity over Platform 1-A. Platform 1-B represents a stiffened plate/shell and consists of a representative aircraft stiffened skin with riveted stringers, manufactured with different materials. However, this methodology relies on the availability of an accurate FE model. In practice, the original equipment manufacturer (OEM) usually has a validated FE model that they use to compute stresses and strains.

In the case of the CF-188, the estimated loads were based on flight testing, in-service monitoring and parametric load formulation. This approach provides information on load distributions over the entire wing structure, and has been proven sufficient to provide a good estimation on a complex structure, as shown in [23]. The fatigue testing and subsequent application of residual strength static tests to the CF-188 wing [24], in the test end configuration, to 120% of the design limit load and to the 150% design limit or ultimate wing root bending loading with induced damage, provided the required substantiation for operation of the inner and outer wing for 6000 flight hours of RCAF and Royal Australian Air Force (RAAF) usage. For this determination, test engineers attempted to apply the same loads, both in magnitude and distribution, that the structure experienced in service [25]. Large numbers of different load conditions are seen in actual service and measured load spectra can contain thousands if not many hundreds of thousands of different load conditions [26]. These loads are generally provided to the test engineer as a set of section loads (shears, moments and torques) for a large number of locations on the structure. Thus, for the wing example, the test engineer would have received curves of shear, moment and torque as a function of wing span. These distributed loads, derived through flight testing, fleet usage data reduction and complex parametric load formulations must then be applied to the test article in a full scale test to prove the structure is capable of meeting its life objective. In a full scale test, a finite number of hydraulic actuators are connected to whiffle trees, consisting of a series of beams and links, to distribute the actuator loads to a larger number

of loading locations on the test article. It is not possible to match every measured load condition exactly, unless there are a very limited number of load conditions or a very large number of actuators. With the limited number of actuators and the whiffle tree geometry being fixed once designed, some form of optimization is typically required to get the 'best' match to the target loads for every load case. A number of techniques have been used in full scale test applications, though, in general, the process consists of minimizing the errors between the calculated and target loads for every load station [27]. As long as these section loads are matched, it is generally assumed that the load distribution will be adequately represented. Unfortunately, due to all the assumptions made during the flight testing, usage data reduction, parametric load formulations and optimizations to minimize errors, the test engineer is fortunate if the loads are within ±5% of the targeted parametric load formulation estimates. In the case of the CF-188 wing test, errors of up to 20% occurred for some load conditions; however, these represented only 0.2% of the load cases that could not be optimized initially. This highlights the requirement for developing a reliable aircraft deployable load monitoring system that one day could be installed on every aircraft for individual aircraft load monitoring.

6. Conclusions

The use of MEMS for load monitoring as an inverse problem has been assessed. The results demonstrate that it is feasible to accurately estimate strains and shear forces on a simple structure. It was also shown how strain distribution in complex structures may be obtained through the use of an accurate FE model in combination with an accurate displacement surface obtained from the integration of a surface fit to the measured MEMS slope data. The combination of a FE model with a displacement curve as an input to the model has been shown to provide accurate results when compared to experimental reference strain gauges. More importantly this technique provides strain values in all locations of the structure and is not limited to specific predefined points of interest.

The use of the Euler–Bernoulli approach involved a series of underlying assumptions, which included the prior knowledge of the load application locale in order to divide the structure into different domains with continuous boundary conditions at the interfaces of the domains, i.e., load application point. Although this might seem a large downside, it is important to note that in the case of a complex structure, this might still be necessary in order to take advantage of the simplicity of utilizing an analytical approach, subdividing the complex structure and complex loading and boundary conditions into simpler piecewise representations. In the case that this is not achievable, the deformation of a complex structure can still be obtained without any prior knowledge of the load application point through the use of FE modelling.

Finally, the use of the NRC-IAR developed custom filter, based upon the extended Kalman–Bucy architecture, gave results that demonstrated how mathematical predictive algorithms might aid in the acquisition of better measurements where the level of uncertainty is high. This type of approach could be combined with machine learning technologies to estimate loads through an optimization problem from which different kinds of computational tools could be used to estimate the most likely loading condition for a specific deformation function.

Acknowledgments

This study was funded by the National Research Council of Canada in collaboration with Defence Research Development Canada. Special thanks to Dr. Julio Valdés from the Institute for Information Technology at NRC for his technical support on the statistical aspects of this study.

References

[1] Simpson D L, Hiscocks R J, Zavitz D and Canadair 1991 A parametric approach to spectrum development *AGARD Conf. Proc. on Fatigue Management* AGARD-CP-506, December

[2] Engineeing Sciences Data Unit 1979 Estimation of the endurance of civil aircraft wing structures IHS *Eng. Sciences Data Unit* Data Items #79024, October

[3] Skopinski T H, Huston W B and Aiken W S Jr 1952 Calibration of strain gauge installation in aircraft structures for the measurement of flight loads *N.A.C.A. Report* 1178 August

[4] Design and Airworthiness Requirements for Service Aircraft DEF STAN 00-970 Part 1/5, section 3, P.23

[5] Rugienius A V 1977 The dissection of an aircraft loads spectrum produced by peak-counting accelerometers LTR-ST-951, NAE, November

[6] Wu J, Yuan S, Shang Y and Wang Z 2009 Strain distribution monitoring wireless sensor network design and its evaluation research on aircraft wingbox *Int. J. Appl. Electromagn. Mech.* **31** 17–28

[7] He L, Zhang J and Jia K 2010 Design and research of piezoelectric pump with MEMS flow sensor *Proc. IEEE Conf. of Mechatronics and Automation (ICM)* pp 412–5

[8] Pereyma M, Motyka I and Lobur M 2007 Perspectives of smart RFID tags usage fabricated by MEMS technologies *Proc. IEEE Perspective Technologies and Methods in MEMS Designs* p 113

[9] Ko W L, Richards W L and Tran V T 2007 Displacement theories for in-flight deformed shape prediction of aerospace structures *NASA Report* TP-2007-214612

[10] Inaudi D, Favez P, Belli R and Posenato D 2011 Dynamic monitoring systems for structures under extreme loads *J. Appl. Mech. Mater.* **82** 809

[11] Lee H 2001 Development of a hybrid uni-axial strain transducer for rail applications *Internal Report* (Washington, DC: Transportation Research Board, National Research Council) http://onlinepubs.trb.org...ail/hsr-15final_report.pdf (last accessed April 24th 2012)

[12] Meyer J, Bischoff R and Feltrin G 2009 Microelectromechanical systems (MEMS) *Encyclopedia of Structural Health Monitoring* (New York: Wiley)

[13] Prime M B 2001 Cross sectional mapping of residual stresses by measuring the surface contour after a cut *Trans. ASME* **123** 162–8

[14] Prime M B 2009 The contour method: a new approach in experimental mechanics *Proc. SEM Annual Conf.* (*Albuquerque, NM*)

[15] Renaud G, Rutledge R S and Hiscocks R J 2005 Development of CF-18 wing finite element model—residual strength test modeling LTR-SMPL-2005-0037
[16] Renaud G, Rutledge R S and Hiscocks R J 2005 Development of CF-18 wing finite element model—phase II LTR-SMPL-2005-0030
[17] Popov E P 1990 *Engineering Mechanics of Solids* (Englewood Cliffs, NJ: Prentice-Hall)
[18] Kuipers J B 1999 *Quaternions and Rotation Sequences* (Princeton, NJ: Princeton University Press) ISBN: 0-691-05872-5
[19] Crisfield M A 1991 *Nonlinear Finite Element Analysis of Solids and Structures* (West Sussex, England: Wiley)
[20] Martinez M, Rocha B, Li M, Beltempo A, Yanishevsky M and Rutledge R S 2011 Micro-electro-mechanical systems (MEMS) for static and quasi-static load monitoring applications LTR-SMPL-2011-0222
[21] Davis J C 1986 *Statistics and Data Analysis in Geology* 2nd edn (New York: Wiley)
[22] Gallant A R and Fuller W A 1973 Fitting segmented polynomial regression models whose join points have to be estimated *J. Am. Stat. Assoc.* **68** 144–7
[23] Rutledge R S, Hiscocks R J, Christie A, LeBlanc R and Cloutier S 2009 CF-18 IFOSTP FT245 Wing test: final report and damage summary LTR SMPL 2009-0160
[24] Rutledge R S, Renaud G, Hiscocks R J, Backman D and Christie A 2007 FT245 Wing test: residual strength test report LTR-SMPL-2007-0046
[25] Hiscocks R J, Rutledge R S and Hewitt R L 2000 Calculation of actuator loads for full-scale aircraft fatigue testing *21st Symp. of the Int. Committee on Aeronautical Fatigue* Toulouse, France, CPR-SMPL-2000-0206
[26] Hewitt R L 1998 Full-scale aircraft fatigue testing—sandbags to simulation *Proc. Int. Conf. on Mechanical Testing of Materials and Structures (English Ed.)* ed S Lee, J W Tang and D S M Chor (Hong Kong: The Hong Kong University of Science and Technology) pp 1–42
[27] Hewitt R L and Rutledge R S 1994 Computer applications in full-scale aircraft fatigue tests *Automation in Fatigue and Fracture: Testing and Analysis, ASTM STP 1231* ed C Amzallag (Philadelphia: American Society for Testing and Materials) pp 51–69